A new $Na_{0.5}Bi_{0.5}TiO_3$ based lead-free piezoelectric system with calculated end-member $Bi(Zn_{0.5}Zr_{0.5})O_3$

Feng Liu[a,b], Olivia Wahyudi[a], Yiqing Lu[a], Yongxiang Li[a,*]

[a]The Key Laboratory of Inorganic Functional Materials and Devices, Shanghai Institute of Ceramics, Chinese Academy of Sciences, Shanghai 200050, China
[b]University of Chinese Academy of Sciences, Beijing 100049, China

Abstract

This study shows a new lead-free piezoelectric system $(1-x)Na_{0.5}Bi_{0.5}TiO_3–xBi(Zn_{0.5}Zr_{0.5})O_3$ [$(1-x)NBT–xBZZ$, x=0, 0.02, 0.03, 0.035, 0.04 and 0.05]. The structure of $Bi(Zn_{0.5}Zr_{0.5})O_3$ was calculated with first-principles method. A morphotropic phase boundary (MPB) near x=0.03 between rhombohedral and pseudo-cubic phases was found, and its improvement in electrical properties was demonstrated. In the MPB composition, the maximum polarization, remnant polarization, coercive field and piezoelectric coefficient are $46.4\ \mu C/cm^2$, $39.2\ \mu C/cm^2$, 4.8 kV/mm and 95 pC/N, respectively. The results not only show a new lead-free piezoelectric system but also suggest a new route to designing lead-free piezoelectric materials.
© 2015 Elsevier Ltd and Techna Group S.r.l. All rights reserved.

Keywords: Lead-free; MPB; NBT–BZZ; First-principles

1. Introduction

Due to the environmental concerns over the toxicity of lead, the search for lead-free piezoelectrics has been the subject of much research over the last decade [1]. There are many promising perovskite-based lead-free piezoceramics, among which the $Na_{0.5}B_{0.5}TiO_3$ (NBT) based ceramics, are considered to be excellent candidates due to their large ferroelectric remnant polarization $P_r=38\ \mu C/cm^2$ and high Curie temperature $T_C=320\ °C$ [2]. However, the high coercive field and high conductivity of pure NBT ceramics have made it difficult for practical applications. Thus, many works have focused on improving the piezoelectric properties of NBT ceramics by adding $BaTiO_3$ (BT), $Na_{0.5}K_{0.5}NbO_3$ (KNN) and other perovskite oxides to form solid solutions, especially those exhibiting the so-called morphotropic phase boundary (MPB) [3–7]. At the MPB, composition-induced phase transitions occur and the co-existence of two different phases results in a significant enhancement in the piezoelectric properties of NBT.

Recently, tetragonal $Bi(Zn_{0.5}Ti_{0.5})O_3$ (BZT) has been theoretically calculated from first principles for its outstanding properties such as high tetragonality, c/a ratio of 1.21 and large ferroelectric polarization of $150\ \mu C/cm$ [8–11]. Although pure BZT can only be synthesized under high pressure, many studies have demonstrated that BZT-containing solid solutions can be stable in ambient pressure and show improved ferroelectric properties [12–14]. However, all these theoretical works are based on the fact that $Bi(Zn_{0.5}Ti_{0.5})O_3$ has been experimentally proven to exist [15]. It is unclear that the theoretical prediction and phase boundary construction can still work without the existing experimental foundations.

In this study, we designed a new ferroelectric system with $Bi(Zn_{0.5}Zr_{0.5})O_3$ (BZZ) as the end-member, with prior theoretical calculation of BZZ. As expected, it is not possible to prepare pure BZZ by using an ordinary solid-state synthesis route, already observed for BZT and $Bi(Mg_{0.5}Ti_{0.5})O_3$ (BMT) [15,16]. However, it is an excellent end-member to form new lead-free pseudo-binary solid solutions due to its high tetragonality, as observed from our theoretical calculation results. With this motivation, solid solutions of lead-free NBT and BZZ, with compositions of $(1-x)NBT–xBZZ$ with x=0, 0.02,

*Corresponding author.
E-mail address: yxli@mail.sic.ac.cn (Y. Li).

0.03, 0.035, 0.04 and 0.05 were prepared, and their structures as well as their electrical properties were investigated.

2. Experimental procedure

The plane wave pseudopotential methodology as implemented in the CASTEP code is used in this work. The Perdew–Burke–Emzerhof (PBE) generalized gradient exchange correlation functional is employed together with PBE-generated ultra-soft pseudo-potentials for Bi, Zn, Zr, Ti and O. The plane wave cut-off energy was set to 450 eV. The Brillouin zone was sampled by $10 \times 10 \times 5$ k-point mesh. As shown in Fig. 1, we employed a $a \times a \times 2c$ supercell (artificial supercell structure) to model BZZ and BZT, where the experimental lattice constants of a and c of BZT are used as starting structure parameters [14]. The supercell contains 10 atoms, where the B-site Zn and Zr (Ti in BZT) ions are ordered along the [001] direction. To obtain the theoretical equilibrium structure for BZZ and BZT, both the lattice constants (a and c) and the atomic positions were optimized within the framework of a tetragonal symmetry (space group P4mm). Since there is no experimental data of BZZ, the starting structural parameters used in the calculation was designed based on the BZT structure. In order to illustrate the structural differences between BZZ and BZT, both BZZ and BZT structures were relaxed under the same calculation conditions.

Ceramic samples of $(1-x)$NBT–xBZZ ($x=0$, 0.02, 0.03, 0.035, 0.04 and 0.05) were prepared by a solid state reaction method. The starting raw materials were Bi_2O_3 (99.999%), Na_2CO_3 (99.8%), TiO_2 (99.3%), ZnO (99.0%), and ZrO_2 (99.9%). The carbonates were dried prior to mixing to remove moisture. For each composition, the starting materials were weighed according to the respective stoichiometric formula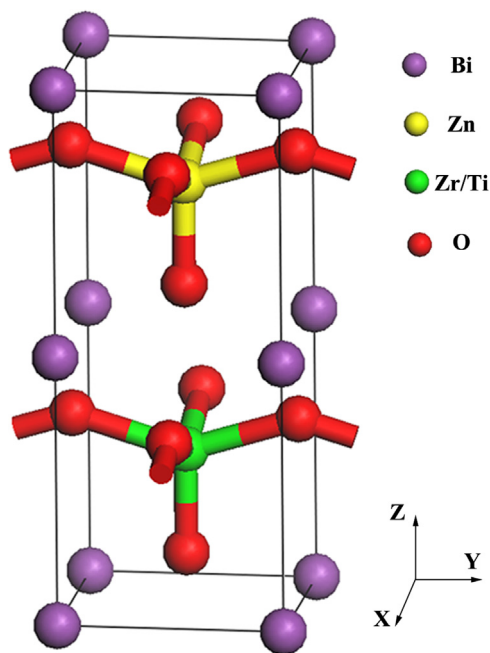, and mixed by ball milling using zirconia balls in ethanol medium for 6 h. The dried powders were then calcined at 850 °C for 3 h and ball milled again for another 6 h. The powders were subsequently pressed into green disks with a diameter of 16 mm under uniaxial pressure of 60 MPa. These pellets were then sintered at 1120–1180 °C in air.

XRD measurements were carried out on unpoled sintered samples using a Bruker D8 Advance diffractometer in Bragg–Brentano geometry. All data were collected in the 2θ range of 10–80° with a step width of 0.02° at room temperature. Le Bail refinements were carried out using the Fullprof software package [17]. The peak profiles were modeled with T-C-H pseudo-Voigt function [18] which is convoluted with asymmetry due to axial divergence while the backgrounds were refined using a linear interpolation between graphically selected points.

For electric measurements, the surfaces of the pellets were coated with a thin layer of silver paste and fired at 700 °C for 30 min. The temperature dependent dielectric constant (ε_r) and loss tangent ($\tan \delta$) of unpoled disks were measured at different frequencies (1 kHz to 1 MHz) using an impedance analyzer (Wayne Kerr 65320B) in a temperature range from 50 to 400 °C. Electric measurements were carried out at room temperature in silicone oil. The hysteresis loops (P–E) were measured at 10 Hz by Precision premier II (Radiant Tech. USA). The piezoelectric coefficient (d_{33}) was measured using Berlincourt-d_{33}-meter (Institute of Acoustic, Chinese Academy of Sciences, ZJ-6A, Beijing, China). Wayne-Kerr 65320B impedance analyzer was used to measure the first resonance and anti-resonance frequencies of poled samples (poling field 6 kV/mm) and the planar electromechanical coupling factor (k_p) were evaluated on the basis of IEEE standards (ANSI/IEEE Std. 176-1987).

3. Results and discussion

The optimized lattice parameters of BZZ and BZT are presented in Table 1, together with the experimental BZT values taken from the literature [15]. The most energetically favorable lattice parameters calculated for BZZ are $a=3.831$ and $c=5.060$ Å, about 0.2% and 9.3% more than the experimental results of BZT, respectively. On one hand, the atomic radius of Zr ($r_{Zr}=1.60$ Å) is larger than Ti ($r_{Ti}=1.47$ Å), which increases the values of both a and c lengths. On the other hand, the energetic stabilization effect decreases a and increases c lattice parameters, as can be seen from the calculated and experimental BZT structures. The calculated tetragonality of BZZ, $c/a=1.321$, is larger than calculated value of BZT $c/a=1.302$. It is noted that the tetragonality is

Fig. 1. The schematic structure of BZZ and BZT.

Table 1

The calculated lattice parameters *a*, *c* (Å), tetragonal *c/a* and equilibrium volume *V* (Å³) of BZZ and BZT. The experimental values of BZT are also given.

	a (Å)	c (Å)	c/a	V
BZZ	3.831	5.060	1.321	74.26
BZT	3.770	4.910	1.302	69.80
Expt.	3.822	4.628	1.211	67.60

related to the phase boundary composition, larger tetragonality will lead to a phase boundary composition with smaller content of the tetragonal end-member. Thus, the value of BZZ content in $(1-x)$NBT–xBZZ at phase boundary composition is expected to be lower than 0.0375, the corresponding BZT addition in NBT–BZT lead-free system [13]. Also, the difference in calculated and experimental values of BZT is reasonable and our calculated values are consistent with other theoretical studies [10,11], suggesting the accuracy of our calculation method.

Fig. 2 shows the XRD patterns with different x values. Superstructure peaks marked with asterisk were observed for the x=0 to 0.02 patterns, indicating the presence of R3c phase [13]. A careful examination of the XRD patterns at $2\theta=48°$ reveals a phase boundary at around x=0.03 and thus, patterns at x=0 was refined with rhombohedral symmetry belonging to R3c space group. In contrast to the anticipated tetragonal structure, due to the limits of our XRD data, we do not find any evidence of a lower symmetry other than the cubic symmetry for x=0.04 and x=0.05 compositions. Indeed, in the literature, we can find other diffraction studies having difficulties in resolving the structure around the reported MPB composition due to the slight non-cubic distortion which is hard to resolve through diffraction techniques [19,20]. Therefore, patterns when x=0.04 and x=0.05 were refined with cubic $Pm\overline{3}m$ space group while x=0.02, 0.03 and 0.035 were refined as a mixture of $Pm\overline{3}m$ and R3c phases. When the amount of BZZ was increased, mainly when x=0.035, 0.04

and 0.05, there were peaks belonging to impurity phase of ZrO_2 and therefore ZrO_2 phase was also included in the refinements.

Anisotropic peak broadening model [21] was also used in for the full-profile fitting of rhombohedral phase where peaks are broader. However for x=0.02 pattern, this model is not sufficient in describing the profile, as seen from the relatively higher R-factor values. This may be due to the presence of local monoclinic domains, as observed in the widely studied lead-based MPB ceramics [22]. In practice, it is difficult to refine using the rhombohedral structure because of its unusual axes direction. Thus, the rhombohedral cell is referred to the hexagonal coordinate system. The lattice parameters as a function of x values are tabulated in Table 2 and shown in Fig. 3 where the shaded region indicates MPB region. The unit cell parameters of the hexagonal system (R3c phase) in Table 2 are converted to the equivalent rhombohedral cell in Fig. 3 for ease of comparison. As observed in Fig. 3, a large variation in lattice parameters is observed at the MPB region when x=0.03.

Table 3 shows the physical and dielectric properties of $(1-x)$NBT–xBZZ at room temperature. All specimens exhibited more than 95% relative densities. The relative density increases from 95% for x=0 (pure NBT) to 98% for x=0.03, then slightly decreasse to 97% for x=0.04. This suggests the MPB shows improved sintering property in NBT-based
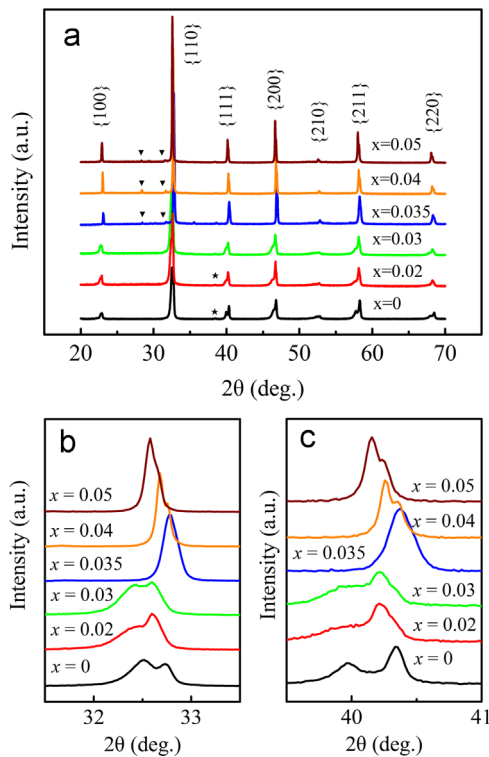

Fig. 2. (a) XRD patterns of the piezoceramics, the asterisks indicate the superstructure peak corresponding to the space group of *R3c* and the arrows on patterns of x=0.035–0.05 indicate the ZrO_2 peaks. (b) and (c) details of composition dependent XRD patterns.

Table 2
Results from the Le Bail fit showing the lattice parameters and the reliability factors.

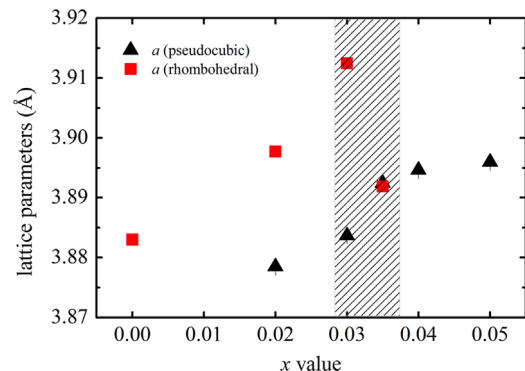| x value	Space group	a(Å)	c(Å)	R_p (%)	R_{wp} (%)	χ^2
0	R3c	5.4805(1)	13.5038(2)	9.54	7.85	3.30
0.02	R3c	5.5292(4)	13.418(1)	19.2	17.0	3.56
	$Pm\overline{3}m$	3.8785(2)				
0.03	R3c	5.5266(3)	13.586(1)	15.8	13.6	2.51
	$Pm\overline{3}m$	3.8836(2)				
0.035	R3c	5.4936(2)	13.5325(4)	13.1	10.6	1.37
	$Pm\overline{3}m$	3.89245(8)				
0.04	$Pm\overline{3}m$	3.89463(5)		15.4	12.2	1.95
0.05	$Pm\overline{3}m$	3.89595(5)		14.7	11.7	1.49

Fig. 3. The variation of lattice parameters as the function of composition.

system. Meanwhile, the specimen for $x=0.03$ also shows an abnormal low dielectric constant which may be related to the MPB.

Fig. 4(a) and (b) shows the temperature dependence of the relative dielectric constant (ε_r) and loss tangent (tan δ) for $(1-x)$NBT–xBZZ ($x=0$, 0.02, 0.03, 0.035, 0.04 and 0.05) at 10 kHz. With the addition of BZZ, there is an increase in the Curie temperature from 315 °C when $x=0$ to 348 °C when $x=0.03$. This improvement of about 30 °C is inferior to some BZT-containing system [12,23]. This is attributed to the low content of BZZ in our system [13]. Meanwhile, both ε_r values at Curie temperature and the depolarization temperature (T_d as indicated by arrow in Fig. 4(b)) tend to decrease with increasing x, which suggests the phase boundary belongs to the MPB(II) between rhombohedral and pseudo-cubic phases rather than typical MPB(I) between rhombohedral and tetragonal phases [7].

The ferroelectric characteristics of $(1-x)$NBT–xBZZ piezoceramics are shown in Fig. 5. Well saturated P–E hysteresis loops
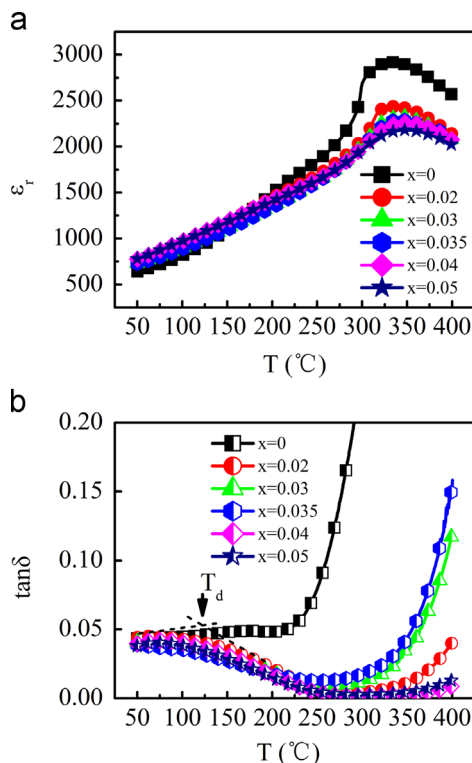
are observed for ceramics with $x \leq 0.035$ and typical results with the composition $x=0$, 0.03 and 0.05 are depicted in Fig. 5(a). The hysteresis loop for the composition with $x=0.05$ tend to be slimmer. Fig. 5(b) summarizes the characteristic properties of all ceramics: maximum polarization P_m at 8.5 kV/mm, remnant polarization P_r and coercive field E_C as a function of BZZ content. As observed, P_m and P_r values increase when $x \leq 0.03$, reach the maximum values at $x=0.03$ with $P_m=46.4$ μC/cm^2 and $P_r=39.2$ μC/cm^2, and then decrease with increasing x content. At the same time, E_C decrease slightly from 5.6 kV/mm when $x=0$ to 4.8 kV/mm when $x=0.03$, indicating that the hysteresis loops tend to be slimmer. This change maybe associated with the fact that the MPB is located near $x=0.03$.

Fig. 6(a) shows the bipolar S–E curves measured at room temperature for the composition with $x=0$, 0.03 and 0.05. When $x=0$ and 0.03, typical butterfly shaped bipolar S–E curves are observed, indicating the ferroelectric nature of the ceramics. However, there is an unusual distortion when $x=0.05$, consistent with the above hysteresis loops. This behavior suggests a FE–AFE transition when $x > 0.03$ [4]. The variation of the maximum positive and negative strain as a function of x, obtained from these S–E curves, is shown in Fig. 6(b). The absolute values of two strains gradually increase, reach the maximum values when $x=0.03$, then decrease notably with increasing x. Unipolar S–E hysteresis curves for the three characteristic compositions are also shown in Fig. 6(c) while the variation of the unipolar strain value with composition is depicted in the inset. The unipolar strain value first increase when $x \leqslant 0.03$ and then decrease with increasing x, consistent with the above bipolar S–E curves. The variation of both bipolar and unipolar S–E curves confirms the existence of MPB near $x=0.03$.

Table 3
The relative density and dielectric properties at room temperature for different composition ceramics.

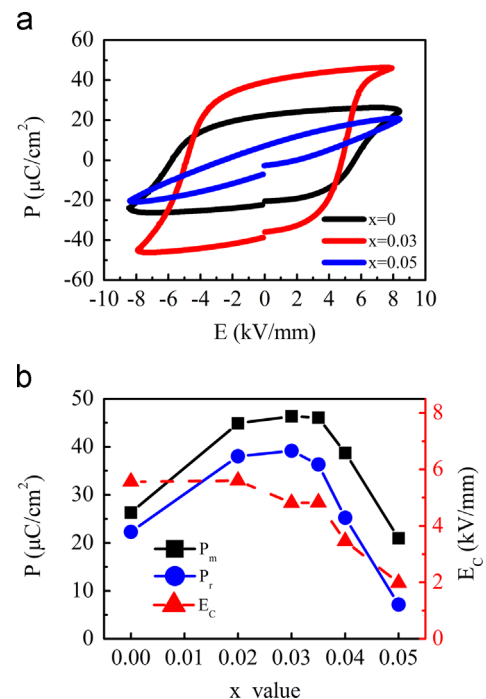| x	0	0.02	0.03	0.035	0.04	0.05
ρ_r (%)	95.4	97.6	98.5	97.4	96.7	98.1
ε_r (10 kHz)	581	682	669	673	711	718
tan δ (%)	4.2	4.2	4.0	4.0	3.8	3.7

Fig. 4. Temperature dependent (a) relative dielectric constant and (b) loss tangent measured at 10 kHz.

Fig. 5. (a) P–E ferroelectric loops of the composition with $x=0$, 0.03 and 0.05 and (b) composition dependent P_m, P_r and E_C.
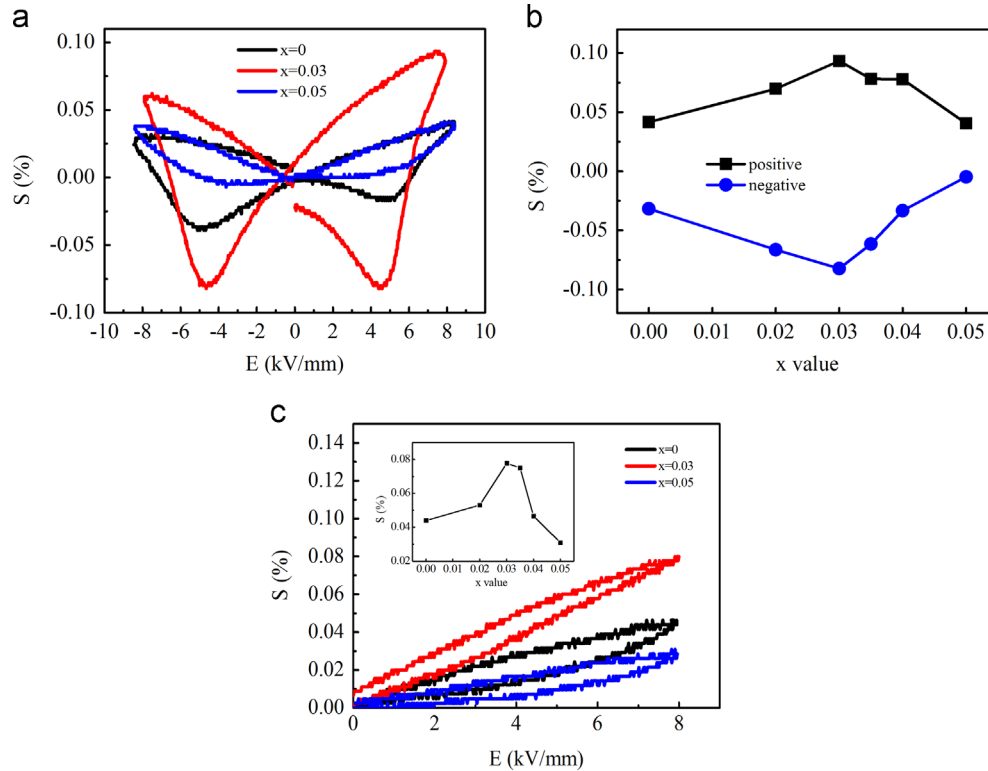
Fig. 6. (a) Bipolar *S–E* curve of the composition with $x=0$, 0.03, 0.05 and (b) composition dependent maximum positive strain and negative strain. (c) unipolar *S–E* curve of the composition with $x=0$, 0.03, 0.05, the inset plots the composition dependent maximum strain value.
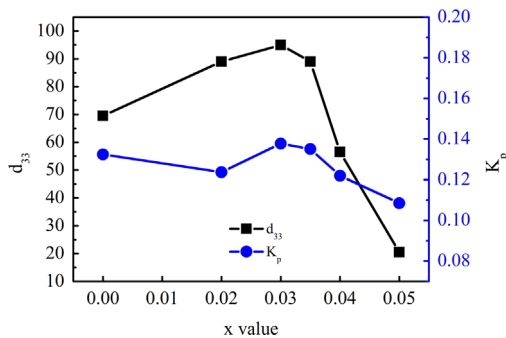

Fig. 7. Piezoelectric coefficient and coupling factor as the functions of composition.

The variation of piezoelectric coefficient (d_{33}) and planar coupling factor (k_p) as a function of x is shown in Fig. 7. The d_{33} and k_p values vary between 21–95 pC/N and 0.11–0.14, respectively. These values are similar with BZT modified NBT piezoceramics but inferior to other NBT-based lead-free systems [3,4,6,24]. The samples of x=0.03 located in the MPB, exhibits highest d_{33} and k_p values of 95 pC/N and 0.14, respectively.

For specimens with x > 0.03, the XRD patterns (Fig. 2) have shown a cubic symmetry. According to point group theory, perovskite-type materials with cubic symmetry do not have spontaneous polarization. Therefore, the above ferroelectric property measurements actually indicate that these specimens do not have a true cubic symmetry, but rather they may possess high structure symmetry approaching the cubic structure, undetected by

our XRD. On the other hand, it has also been shown that a distinct non-cubic distortion can develop out of an apparently cubic symmetry when the materials are exposed to an electric field [20,25]. Thus, the cubic phases are referred here as pseudo-cubic.

4. Conclusions

In conclusion, this study investigates the structure and ferroelectric properties of a new lead-free piezoelectric system, $(1-x)$NBT–xBZZ ceramics. The addition of BZZ allows a phase transition from the rhombohedral phase to a pseudo-cubic phase, thus creating a MPB at around x=0.03. With respect to the electrical properties, the addition of BZZ leads to an improvement of the ferroelectric as well as piezoelectric properties. Our results have shown the possibility of obtaining NBT-based lead-free ceramics with improved ferroelectric properties and large piezoelectricity with the addition of a theoretically tetragonal structure BZZ without prior experimental evidence. This opens the door for the vast possibility in tailoring and designing for new lead-free piezoelectric materials.

Conflict of interest

We declare that we do not have any commercial or associative interest that represents a conflict of interest in connection with the work submitted.

Acknowledgments

References

[1] Y. Saito, H. Takao, T. Tani, T. Nonoyama, K. Takatori, T. Homma, T. Nagaya, M. Nakamura, Nature 432 (2004) 84.

[2] G.A. Smolenskii, V.A. Isupov, A.I. Agranovskaya, N.N. Krainik, Sov. Phys. Solid State 2 (1961) 2651.

[3] T. Takenaka, K. Maruyama, K. Sakata, Jpn. J. Appl. Phys. 30 (1991) 2236.

[4] A.B. Kounga, S.-T. Zhang, W. Jo, T. Granzow, J. Roedel, Appl. Phys. Lett. 92 (2008) 222902.

[5] L. Wu, D. Xiao, D. Lin, J. Zhu, Ping Yu, X. Li, Jpn. J. Appl. Phys. 46 (2007) 7382.

[6] M. Kobune, K. Teraoka, H. Nishioka, H. Yamaguchi, K. Honda Jpn. J. Appl. Phys. 50 (2011) 09ND08.

[7] Y. Hiruma, H. Nagata, T. Takenaka, Jpn. J. Appl. Phys. 48 (2009) 09KC08.

[8] T. Qi, I. Grinberg, A.M. Rappe, Phys. Rev. B 79 (2009) 094114.

[9] S. Ju, G.Y. Guo, J. Chem. Phys. 129 (2008) 194704.

[10] J.-Q. Dai, Z. Fang, J. Appl. Phys. 111 (2012) 114101.

[11] H. Wang, H. Huang, W. Lu, H.L.W. Chan, B. Wang, C.H. Woo, J. Appl. Phys. 105 (2009) 053713.

[12] I. Grinberg, M.R. Suchomel, W. Dmowski, S.E. Mason, H. Wu P.K. Davies, A.M. Rappe, Phys. Rev. Lett. 98 (2007) 107601.

[13] S.-T. Zhang, F. Yan, B. Yang, J. Appl. Phys. 107 (2010) 114110.

[14] E.A. Patterson, D.P. Cann, Appl. Phys. Lett. 101 (2012) 042905.

[15] M.R. Suchomel, A.M. Fogg, M. Allix, H. Niu, J.B. Claridge M.J. Rosseinsky, Chem. Mater. 18 (2006) 4987.

[16] D.D. Khalyavin, A.N. Salak, N.P. Vyshatko, A.B. Lopes N.M. Olekhnovich, A.V. Pushkarev, I.I. Maroz, Y.V. Radyush, Chem. Mater. 18 (2006) 5104.

[17] J. Rodriguez-Carvajal, FULLPROF: a program for Rietveld refinement and pattern matching analysis, in: Proceedings of the Collected Abstracts of the Meeting Powder diffraction, Toulouse, France, 1990, p. 127.

[18] B.V. Laar, W.B. Yelon, J. Appl. Crystallogr. 17 (1984) 47.

[19] R. Ranjan, A. Dviwedi, Solid State Commun. 135 (2005) 394.

[20] J.E. Daniels, W. Jo, J. Roedel, J.L. Jones, Appl. Phys. Lett. 95 (2009) 0332904.

[21] P.W. Stephens, J. Appl. Crystallogr. 32 (1999) 281.

[22] B. Noheda, D.E. Cox, G. Shirane, J. Gao, Z.G. Ye, Phys. Rev. B 66 (2002) 054104.

[23] J. Chen, P. Hu, X. Sun, C. Sun, X. Xing, Appl. Phys. Lett. 91 (2007) 171907.

[24] Y. Hiruma, H. Nagata, T. Takenaka, Appl. Phys. Lett. 95 (2009) 052903.

[25] Q. Zhang, Y. Zhang, F. Wang, Y. Wang, D. Lin, X. Zhao, H. Luo, W. Ge, D. Viehland, Appl. Phys. Lett. 95 (2009) 102904.